HIGH STRAIN RATE SUPERPLASTICITY IN A CONTINUOUSLY RECRYSTALLIZED Al–6%Mg–0.3%Sc ALLOY

T. G. NIEH[1], L. M. HSIUNG[1], J. WADSWORTH[1] and R. KAIBYSHEV[2]

[1]Lawrence Livermore National Laboratory, L-369, P.O. Box 808, Livermore, CA 94551, U.S.A. and
[2]Institute of Metals Superplasticity Problems, Khalturina St. 39, Ufa, Bashkortostan, 450000, Russia

Abstract—The superplastic properties of a cold-rolled Al–6Mg–0.3Sc alloy were studied at temperatures between 450 and 560°C and strain rates between 10^{-4} and 10^{0} s^{-1}. The alloy was observed to exhibit superplasticity over wide temperature (475–520°C) and strain rate ranges ($\sim10^{-3}$–10^{-1} s^{-1}). It was found that the addition of Sc to Al–Mg alloys resulted in a uniform distribution of fine coherent Al$_3$Sc precipitates which effectively pinned subgrain and grain boundaries during static and dynamic recrystallization. In this paper, the microstructural evolution during superplastic deformation was systematically examined using both optical and transmission electron microscopy. Based upon this microstructural examination, a mechanism is proposed to explain the observed high strain rate superplasticity in the alloy. A model is also proposed that describes grain boundary sliding accommodated by dislocations gliding across grains containing coherent precipitates. © 1998 Acta Metallurgica Inc.

1. INTRODUCTION

There is now a great interest in developing highly-formable Al alloys, and in particular Al–Mg based alloys, for application leading to lightweight vehicles. Significant efforts have been made to improve the formability of Al–Mg alloys; Al–Mg is a substitutional solid-solution alloy. At appropriate temperatures and strain rates, this alloy undergoes deformation by a solute-drag mechanism; this mechanism is independent of grain size. The solute-drag mechanism is associated with relatively high strain-rate sensitivities of $m = 0.33$. These relatively high values of $m = 0.33$ are expected to lead to tensile elongations of $\sim300\%$. Examples of such large elongations have, in fact, been experimentally achieved in Al–Mg alloys [1, 2]. These types of elongations are close to those found in superplastic materials. In fact, recent studies have demonstrated the possibility of conducting superplastic-like forming operations with Al–Mg alloys by taking advantage of the enhanced ductility developed during solute-drag controlled deformation [3].

For some applications, however, higher ductilities and faster strain rates than those achievable in solute drag controlled alloys are often desirable. For these cases, the ductilities and strain rates accessible in fine-grained superplastic alloys are required. Superplastic materials generally exhibit high ductility without necking or rupture because of the high strain-rate sensitivity, $m = 0.5$, inherent in grain-boundary-sliding (GBS) process. The grain-boundary-sliding mechanism in metals usually requires a stable grain size of less than 10 μm [4]. In theory, two competing processes, GBS and dislocation slip, can control deformation, as illustrated in Fig. 1 in which the logarithm of the stress is plotted as a function of the logarithm of the strain rate. The two separate processes contributing to GBS and slip are represented as straight lines. The point of intersection (marked $\dot{\varepsilon}_{SPmax}$) represents the maximum strain rate for superplastic flow for a given set of microstructural conditions. As noted on the figure, the principal equations for GBS (governed by grain-boundary diffusion) and for slip can be written as equations (1) and (2), respectively [4, 5]:

$$\dot{\varepsilon}_{gbs} = A_{gbs}\left(\frac{b}{d}\right)^3\left(\frac{D_{gb}}{b^2}\right)\left(\frac{\sigma}{E}\right)^2, \qquad (1)$$

$$\dot{\varepsilon}_{slip} = A_s\left(\frac{\lambda}{b}\right)^3\left(\frac{D_L}{b^2}\right)\left(\frac{\sigma}{E}\right)^8, \qquad (2)$$

where $\dot{\varepsilon}_{gbs}$ and $\dot{\varepsilon}_{slip}$ are the strain rates for GBS and slip, respectively; A_{gbs} and A_s are constants; b is Burgers vector; d is the mean linear intercept grain size; λ is the minimum barrier spacing governing slip creep (typically the interparticle spacing or the grain size); D_{gb} is the grain-boundary diffusivity; D_L is the lattice diffusivity; σ is the stress; and E is the dynamic, unrelaxed Young's modulus. By refining grain size it is possible both to make GBS more facile and to inhibit the slip-creep process thereby increasing the maximum strain rate for superplastic flow. Such a change leads to an increase in the maximum rate for superplastic flow from $\dot{\varepsilon}_{SPmax}(i)$
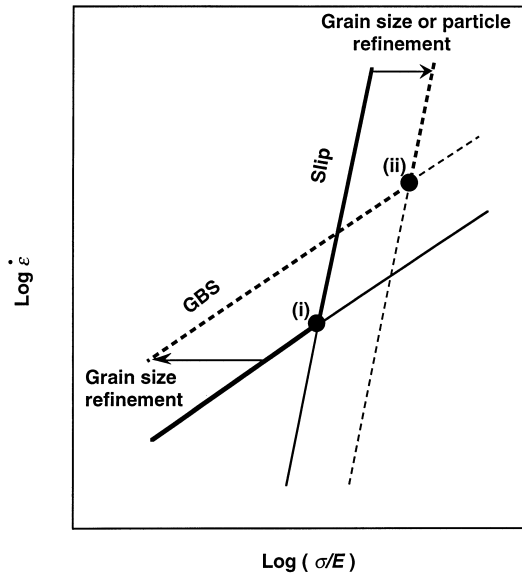
Fig. 1. Two competing mechanisms of GBS and slip. If the structural state is changes so that GBS is enhanced and slip creep is made more difficult, as shown by the dashed lines, the maximum strain rate for superplasticity flow is increased from (i) to (ii).

to $\dot{\varepsilon}_{SPmax}$(ii), as shown in Fig. 1 in which the dashed lines represent a finer grain size condition than the solid lines. Using this concept, Wang *et al.* [6, 7] have studied the microstructure and ductility of a nanocrystalline ($\sim$0.2 μm) Al–3%Mg alloy. The alloy, despite having an initial grain size in the nanometer range, exhibited only limited ductility ($<$200%). The low ductility was attributed to an inability to retain the ultrafine grain size during deformation; grain growth in this alloy was found to be unusually fast even at a relatively low temperature (403 K). Thus, it could be of interest to find an effective grain growth inhibitor for such alloys.

Scandium is the only alloying element to form an equilibrated, thermally-stable, coherent $L1_2$ phase, i.e. Al_3Sc, in aluminum (a phase that is analogous to γ' in Ni-based superalloys). The lattice mismatch between Al_3Sc and Al is only about 1.4%. As a result, the Al_3Sc precipitate is unusually resistant to coarsening. Despite the relatively low solubility of Sc ($\sim$0.38 wt%) and, hence, the limited volume fraction that is available of the Al_3Sc phase, it produces a significant strengthening effect. In fact, Al_3Sc is the most potent strengthener, on an equal atomic fraction basis, known in Al-base systems [8]. The Al_3Sc precipitate is also very effective in stabilizing substructure, thus allowing the use of strain-hardening and grain-boundary strengthening to enhance the strength of Al alloys. For example, Engler and Tempus [9] demonstrated that Al_3Sc precipitates are extremely effective in retarding the onset of recrystallization in an Al–5Mg–Mn alloy (Al 5182).

Creep deformation behavior exhibiting a value of $n = 3$ ($m = 0.33$) can be readily found in coarse-grained Al–Mg-based alloys [1, 4, 10]. For example, the commercial 5083 Al alloy is a Class I solid solution alloy that contains about 4.5% Mg and 0.5% Mn and has a grain size of 25 μm. Other examples are the binary Al–Mg and Al–Sc alloys, and the ternary Al–Mg–Sc alloys reported by Sawtell and co-workers [11]. In their study, a tensile elongation value for an Al–4Mg alloy was found to be about 200%, whereas it was about 1000% for an Al–4Mg–0.5Sc alloy (at 400°C and at strain rates between 10^{-3} and 10^{-2} s^{-1}). The high elongation was attributed to a uniform dispersion of fine Al_3Sc particles in the alloy which greatly refined its grain size. However, the exact roles of Al_3Sc on the subgrain evolution, dislocation- and precipitate-grain boundary interactions, were not clearly identified. Also, the strain rate sensitivity value ($\sim$0.3–0.4) was found to vary with strain rate and temperature, but no mechanism was offered for the observed superplasticity.

Recently, we reported the observation of extended ductility ($\sim$200%) in an Al–6Mg–0.3Sc alloy (designated in the Former Soviet Union as Al 1570) in a thin foil form (0.09-mm thick) [12]. Since tensile elongation is expected to be strongly sensitive to surface defects on thin samples, we predicted that the tensile elongation would be higher if the sample was in a bulk form (e.g. 2-mm thick). The purpose of this paper is to demonstrate the effectiveness of Al_3Sc in stabilizing substructure/structure and thereby producing superplasticity at high strain rates in a bulk Al–6Mg–0.3Sc alloy.

2. EXPERIMENTS

The chemical composition (in wt%) of the alloy used in the present study is Al–5.76Mg–0.32Sc–0.3Mn–0.1Fe–0.2Si–0.1Zn. The alloy was initially produced by ingot casting and was 390 mm in diameter and 790 mm in length. The ingot was homogenized at 520°C for 24 h, isothermally forged along its length to 380 mm at $\sim$390°C and then annealed at 320°C for 1 h. The annealed billet was further sliced for cold rolling and the cold rolling was conducted unidirectionally in parallel to the billet long axis with a constant thickness reduction per pass (0.5 mm) and with a total reduction of 80% (16 passes). Tensile specimens were machined from the final sheet ($\sim$2 mm).

Tensile tests were conducted in air at temperatures between 450 and 560°C, and at strain rates between 10^{-4} and 1 s^{-1}, using a screw-driven Instron machine equipped with a radiant furnace. The variation of the target temperatures was controlled to within $\pm$1°C. Both constant crosshead speed and constant strain rate tests were conducted. In addition, strain rate change tests were also per-

formed to measure the strain rate sensitivity values of the alloy.

Microstructures of both the grip and gage sections of tested specimens were examined using optical metallography and a JOEL-200CX transmission electron microscope operated at 200 kV. TEM foils were sliced from the specimens, and prepared by twin-jet electropolishing in a solution of 60% ethanol, 35% butyl alcohol, and 5% perchloric acid at 15 V and −10°C.

3. RESULTS

3.1. Mechanical properties

The true stress–true strain curves for the Al–6Mg–0.3Sc alloy, tested at an initial strain rate of 1.4×10^{-2} s^{-1} at different temperatures (475–540°C), are shown in Fig. 2. At all temperatures there is an immediate hardening upon loading, followed by an apparent softening. No obvious steady-state flow region was observed. Tensile elongations at over 800% (true strain > 2.2) were found at all testing temperatures. Tensile elongation as a function of temperature (strain rate $= 1.4 \times 10^{-2}$ s^{-1}) is depicted in Fig. 3. It is evident that there exists a wide temperature range (475–520°C) within which the tensile elongation is over 1000%. The elongation value drops rapidly when the testing temperature is near or above the solidus temperature of the alloy (i.e. $> > 550$°C). Specifically, the elongation is only 20% at 560°C. This dramatic reduction in ductility is associated with the presence of an excessive amount of liquid phase, in particular at grain boundaries, which causes grain boundary separation in test samples under tension. In fact, a fractographic study carried out on a sample fractured at 560°C did indicate the presence of liquids on grain boundaries.

The tensile elongation is also noted to vary with strain rate. Shown in Fig. 4(a) is the elongation value of Al–6Mg–0.3Sc samples as a function of strain rate at a testing temperature of 475°C. At this temperature, the maximum elongation was

Fig. 3. Tensile elongation as a function of temperature (strain rate $= 1.4 \times 10^{-2}$ s^{-1}).

recorded at a strain rate of 1.4×10^{-2} s^{-1}. Samples superplastically deformed to different strains at 475°C are shown in Fig. 5. It is noted that the specimens deformed quite uniformly. It is particularly pointed out that final necking of these tested samples was not to a point, as is often observed in Al–Mg alloys deformed by solute-drag mechanisms [13].

The logarithm of flow stress (at a fixed strain of 0.5) is plotted as a function of the logarithm of strain rate in Fig. 6. The strain rate sensitivity value, m, defined in the equation $\sigma = k \cdot \dot{\varepsilon}^m$, shown in Fig. 4(b), varies with both temperature and strain

Fig. 4. (a) The elongation value of Al–6Mg–0.3Sc alloy as a function of strain rate at different temperatures.

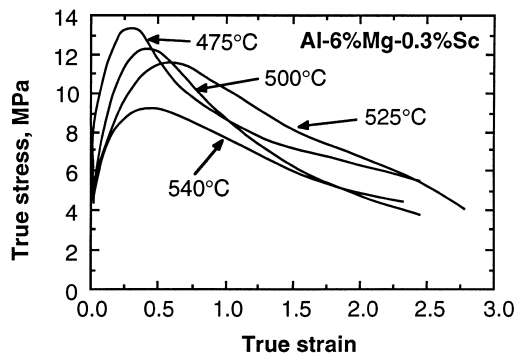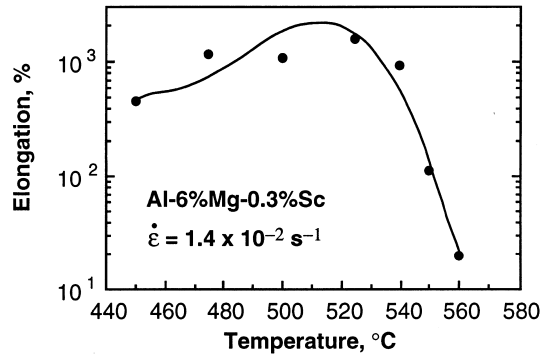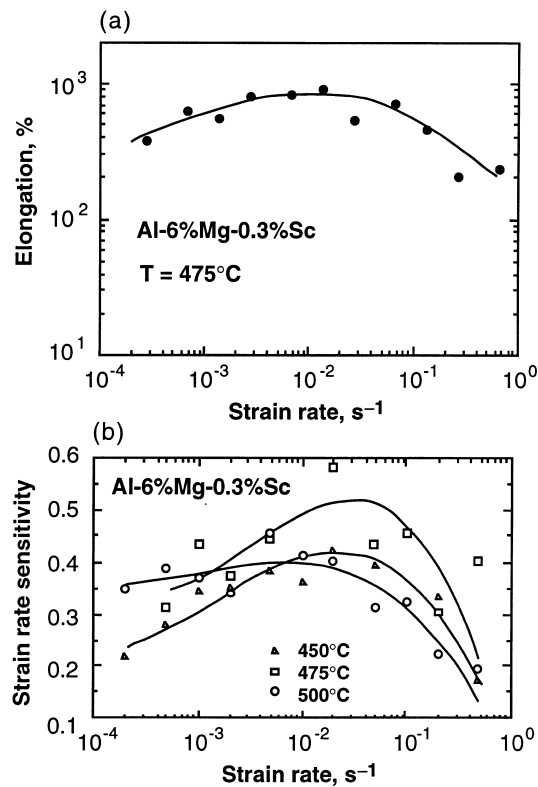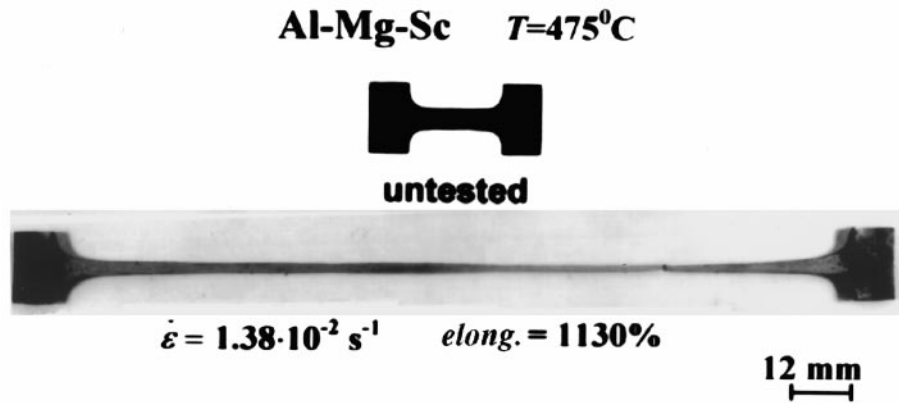

Fig. 2. True stress–true strain curves for the Al–6Mg–0.3Sc alloy tested at an initial strain rate of 1.4×10^{-2} s^{-1} over the temperature range 475–540°C.

Fig. 5. A direct comparison of a superplastically deformed (1130%) Al–6Mg–0.3Sc sample with an untested sample. Uniform deformation along the gage length is evident.

rate. The value of m exhibits a peak at a strain rate of approximately 2×10^{-2} s^{-1} and falls off on both sides, especially in the high strain rate regime. This result is consistent with the data shown in Fig. 4(a), namely, high elongations correspond to high m value. The m value as a function of testing temperature at the optimal strain rate of 2×10^{-2} s^{-1} is shown in Fig. 7. The maximum m value occurs at temperatures of about 500–520°C. This result is again consistent with the data shown in Fig. 3, i.e. high m values result in high tensile elongations. In general, a tensile elongation of over 1000% can be readily obtained at a testing temperature of about 500°C (strain rate $\sim 2 \times 10^{-2}$ s^{-1}).

The activation energy for superplastic deformation, Q, in the Dorn equation:

$$\dot{\varepsilon} = A \cdot (\sigma/E)^n \cdot \exp(-Q/RT) \qquad (3)$$

where R is the gas constant, and T is the absolute temperature, can be calculated from Fig. 8. The calculated activation energy for superplastic Al–Mg–Sc is about 190 kJ/mol which is higher than the activation energy measured for the diffusion of Mg in Al (136 kJ/mol) during creep of Al–Mg alloys [14].
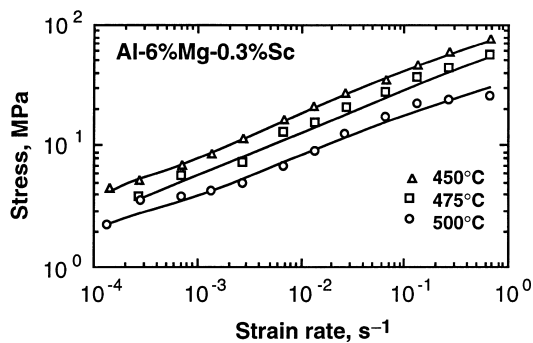
3.2. Microstructure

To examine the microstructural evolution in the alloy during superplastic deformation of Al–6Mg–0.3Sc interrupted tests were systematically carried out at the optimal strain rate of 1.4×10^{-2} s^{-1} and at 475°C. TEM specimens were subsequently prepared from samples deformed to strains of 22%, 110%, 230%, 570%, and 1130% (Fig. 5), respectively.

The microstructure of the starting material is shown in Fig. 8. This microstructure is typical of a heavily-deformed metal, consisting of dislocation cells of size ranging from 200 nm to as large as 1 μm. Some subgrains exist but are rarely seen. The presence of L1$_2$–Al$_3$Sc precipitates was also occasionally detected in some areas, but the amount was insignificant.

The microstructure of the sample deformed to 22%, as shown in Fig. 9(a), primarily consists of grains (or subgrains) with misorientation angles less than 4–5°. The diameter of these grains is estimated to be ~ 3 μm. It is noted that dislocation cells no longer exist and the dislocation density is also greatly reduced. However, significant amounts of Al$_3$Sc precipitates are present, as revealed in Fig. 9(b). These precipitates are of spherical shape

Fig. 6. The logarithm of flow stress (at a fixed strain of 0.5) as a function of the logarithm of strain rate.
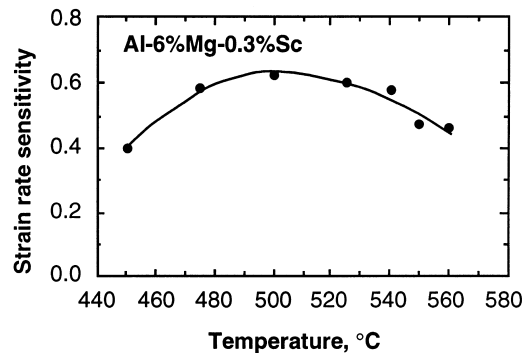

Fig. 7. Strain rate sensitivity as a function of temperature for Al–6Mg–0.3Sc.
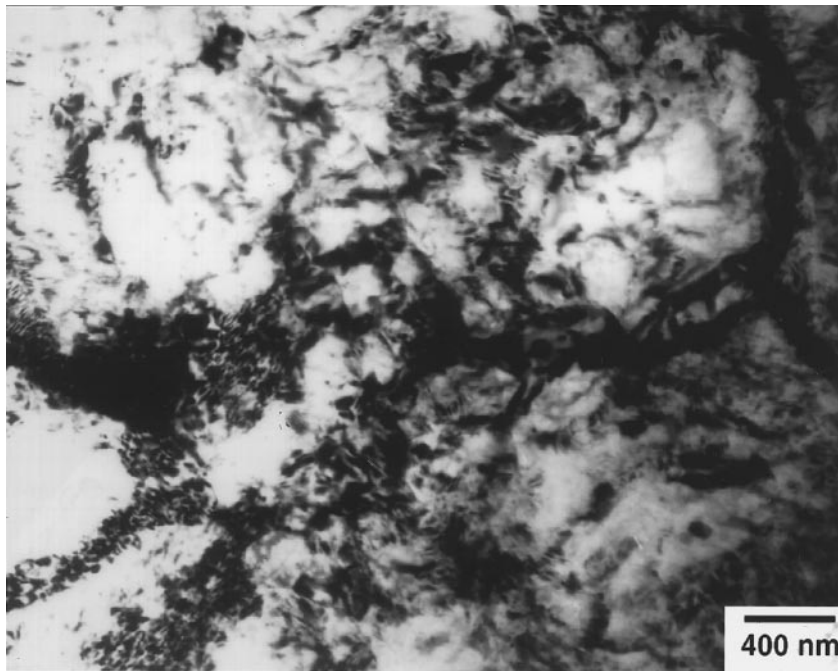
Fig. 8. Microstructure of cold-rolled Al–6Mg–0.3Sc alloy.

and extremely fine, ranging from 5 to 100 nm. A straightforward XRD analysis confirms that they are coherent with the Al matrix. Also noted in Fig. 9(a) is the fact that these coherent Al₃Sc precipitates are quite effective in pinning subgrain boundaries.

After deforming to 110%, many low-angled boundaries were converted into high-angled ones (Fig. 10). Fine Al_3Sc precipitates are found to be very effective in pinning these high-angled grain boundaries. The average diameter of these grains is about 5 μm. It is particularly pointed out that, in addition to fine Al_3Sc precipitates, Fe- and Mn-rich coarse inclusions ($\sim$2–3 μm in diameter) as indicated in Fig. 10(b) were also observed and found to reside at grain boundaries, indicating they also play

an important role in grain boundary pinning. At a yet greater deformation of 230%, the grain boundaries were mainly high-angled and the grain size became slightly larger ($\sim$4–5 μm) than in the 110%-deformed sample. A prevalent feature in some grain interiors is the precipitate–dislocation interaction, as shown in Fig. 11. In the 570%-deformed sample, grain boundaries are essentially high-angled. While Al_3Sc particles are still quite effective in pinning grain boundaries, their density and size are notably increased.

The microstructure of the 1130%-deformed sample, shown in Fig. 12, consists of a fully recrystallized microstructure in which nearly all grain boundaries are high-angled. The average grain size is approximately 8 μm. From a superplasticity point
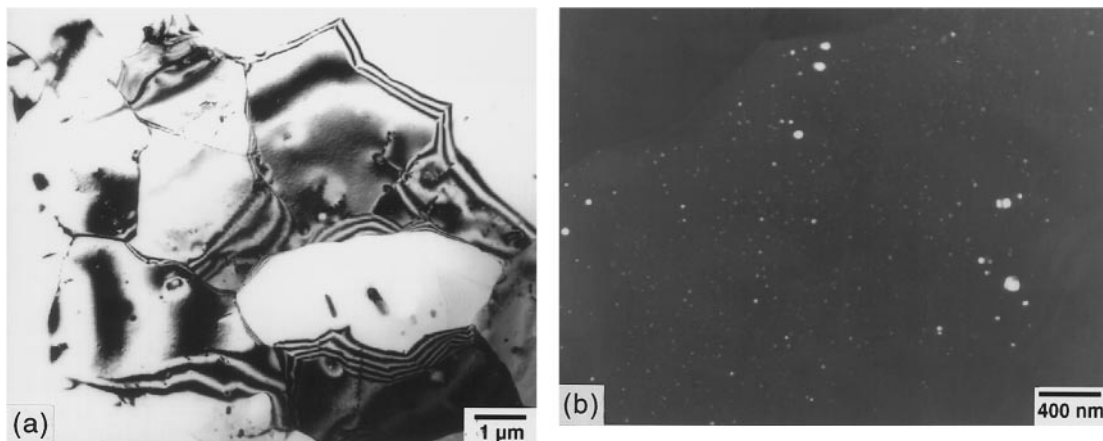

Fig. 9. (a) Microstructure of Al–6Mg–0.3Sc sample deformed to 22% at 475°C and at a strain rate of $1.4 \times 10^{-2}\,\mathrm{s}^{-1}$ and (b) significant amounts of fine Al_3Sc precipitates begin to appear.
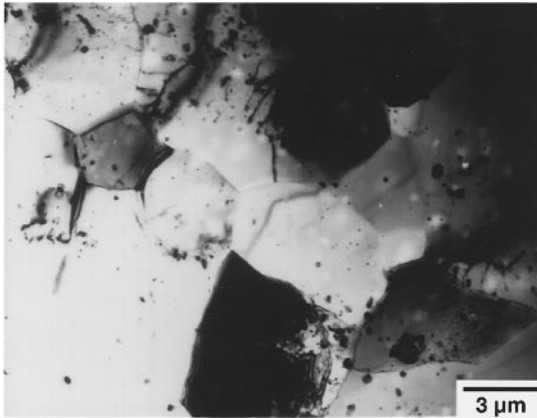
Fig. 10. Microstructure of deformed (110%) Al–6Mg–0.3Sc alloy. Many low-angled boundaries have been converted into high-angled ones.
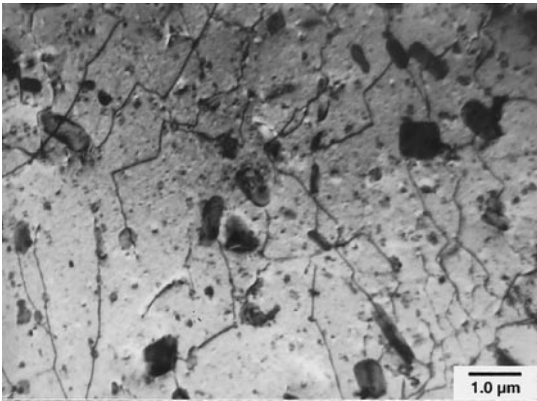

Fig. 11. Al$_3$Sc–dislocation interaction in Al–6Mg–0.3Sc alloy during high temperature deformation.

of view, an 8-μm grain size is still considered to be fine for aluminum alloys. The retention of a fine grain size is attributed to the presence of Al$_3$Sc precipitates. However, the size of the Al$_3$Sc particles in the 1130%-deformed sample is noted to have increased significantly. In actual fact, some coarse (~0.15 μm) Al$_3$Sc are now so large that the Al$_3$Sc–
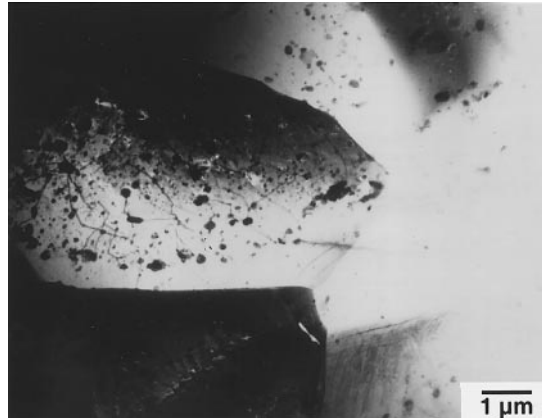

Fig. 12. Microstructure of the Al–6Mg–0.3Sc alloy deformed 1130%.

Al matrix interface is no longer coherent. In contrast to the deformed microstructure, the microstructure in the grip region is considerably different. The microstructure from the grip region (representing a static anneal at 475°C for 45 min) is shown in Fig. 13. Grains are noted to be elongated along the sample direction (i.e., the original rolling direction) and have a lateral dimension of about 4–5 μm. Each grain actually consists of many fine equiaxed subgrains. The diameter of these subgrains is about 1 μm and the misorientation angle measured from the diffraction pattern shown in Fig. 13(b) is less than 4°.

3.3. Cavitation and fracture

In the Al–6Mg–0.3Sc alloy, superplastic deformation induces only limited cavitation. A series of cross-sectional views from different areas in the sample deformed to 1130% is shown in Fig. 14. Discrete cavities can be observed, but no transverse cavity interlinkage is found (Fig. 15). Most of the cavities are observed to align in the stress direction and form stringers, suggesting a mechanism of plasticity-controlled cavity growth. This result is similar to that observed in an Al–4%Mg–
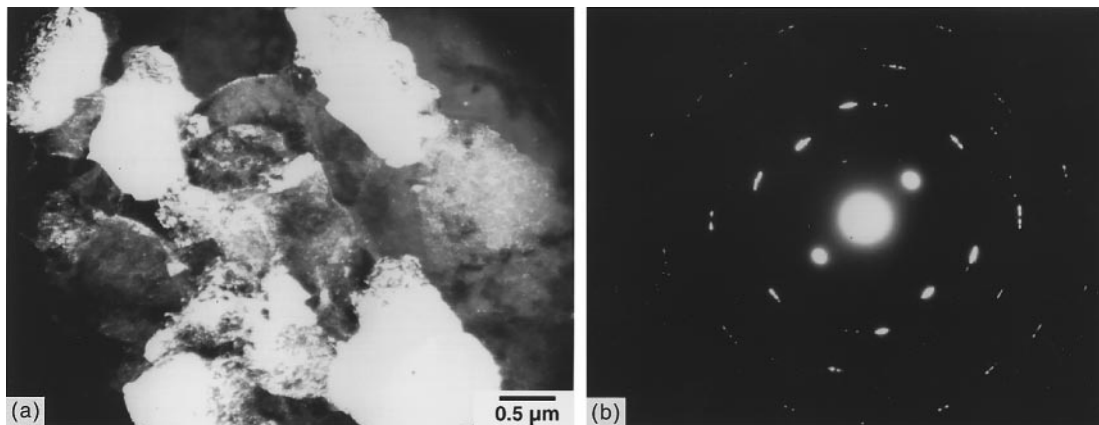

Fig. 13. (a) Microstructure of Al–6Mg–0.3Sc statically annealed at 475°C for 45 min. (b) Diffraction pattern showing that the misorientation angles between subgrains are small (<4°).
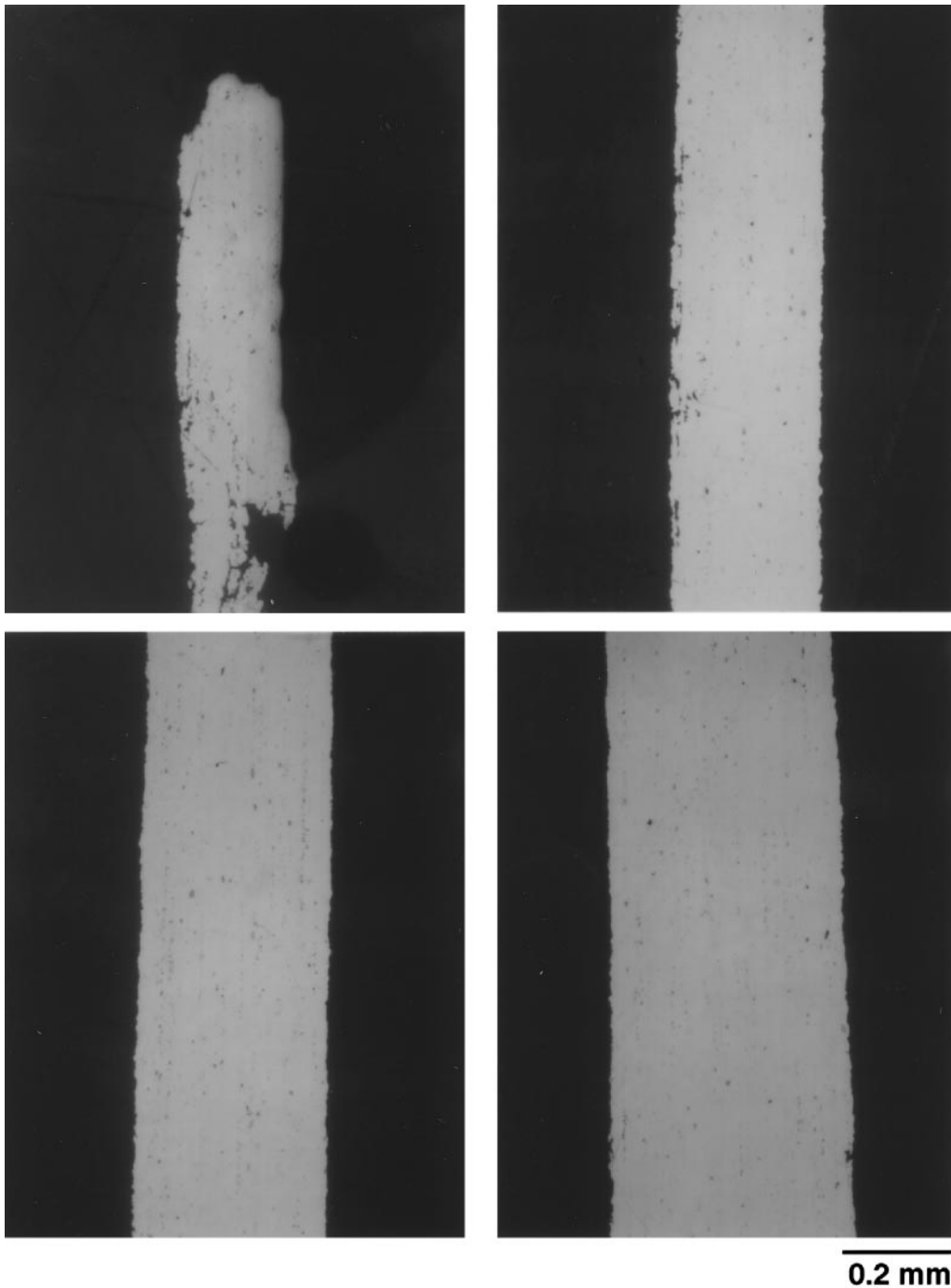
0.2 mm

Fig. 14. Cross-sectional view from different locations of the sample deformed to 1130%. Limited cavitation is observed.

0.5%Sc alloy [11]. Also, it is readily seen that the areal fraction of cavities is low (∼1%). It is pointed out that most of the dark phases in Fig. 14 are in fact, impurity inclusions. Etched microstructures reveal that grains in the deformed area are equiaxed and the grain size near the fracture tip is about 7 μm which is consistent with the TEM observation (Fig. 12). Optical metallography from the grip region also confirms that grains are

elongated along the sample direction (i.e. the original rolling direction).

The fracture surface of a superplastically-deformed Al–6Mg–0.3Sc sample is shown in Fig. 16 (fracture strain = 1130%). It is an intergranular fracture. There is no evidence of grain tearing, indicating fracture was not controlled by macroscopic neck instability, as often observed in coarse-grained Al–Mg-based alloys [1, 4, 10]. Again, it is noted that
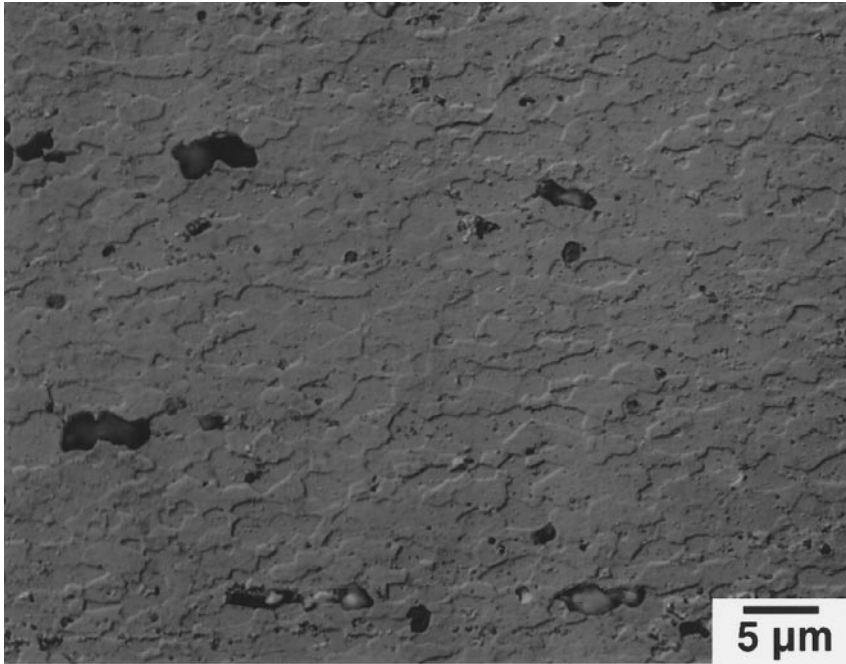
Fig. 15. Discrete cavities are observed but no extensive cavity interlinkage is found.

grains are equiaxed, uniform, and with an average size of about 7 μm.

4. DISCUSSION

The recrystallization and thermomechanical behavior of Al–6Mg–0.3Sc is somewhat similar to that of the commercial Supral alloys (Al–Cu–Zr). For example, static annealing of Supral alloys in the temperature range of 450–500°C results in a stable well-recovered subgrain structure [15]. Even annealing at 500°C only causes the subgrain size to increase from 1.2 μm to 1.5 μm, with an average boundary misorientation of about 5°. This is comparable with that observed in the present Al–6Mg–0.3Sc alloy, namely, an average subgrain size of

Fig. 16. Fracture surface of the superplastically-deformed Al–6Mg–0.3Sc alloy is intergranular (fracture strain = 1130%).

about 1 μm and an average misorientation angle of less than 4° were developed after annealing the alloys at 475°C [Fig. 13(b)]. For Supral alloys the grain stabilizer is fine Al_3Zr, but in Al–6Mg–0.3Sc the granstabilizer is fine Al_3Sc precipitates. Both Al_3Zr and Al_3Sc precipitates have an $L1_2$ structure which is coherent with the Al matrix. The maximum solid solubilities of Sc and Zr in Al are estimated to be 0.38 [11] and 0.15% [16] by weight, respectively.

The fact that the microstructure of the deformed region (Figs 10 and 12) consists of high-angled grains, but the undeformed region (Fig. 13) contains only low-angled subgrains, indicates that concurrent straining and annealing causes an increase in boundary misorientation, i.e. continuous recrystallization takes place. Additional evidence for the occurrence of continuous recrystallization is found in the plastic flow behavior of the Al–6Mg–0.3Sc alloy deformed at a constant strain rate. As shown in Fig. 2, the strain rate continuously decreases during a constant crosshead speed test. Although the starting strain rate was $10^{-2}\,s^{-1}$, it is pointed out that the true strain rate near the end of each test shown in Fig. 2 is, in fact, only about $10^{-3}\,s^{-1}$. This decrease in strain rate can contribute to a certain degree to the apparent decrease in flow stress. To investigate the true plastic flow in the alloy, constant true strain rate tests were subsequently carried out. The true stress–strain curves obtained at a constant strain rate of $1.4 \times 10^{-2}\,s^{-1}$ and at three different temperatures are depicted in Fig. 17. Dynamic strain softening, which is typical of continuous recrystallization, is readily observed in the figure. It is noted that the less-pronounced softening
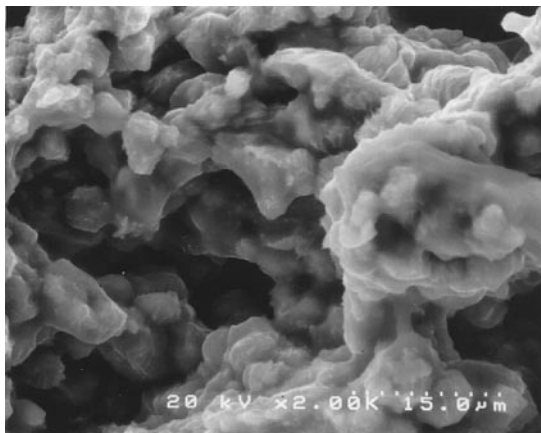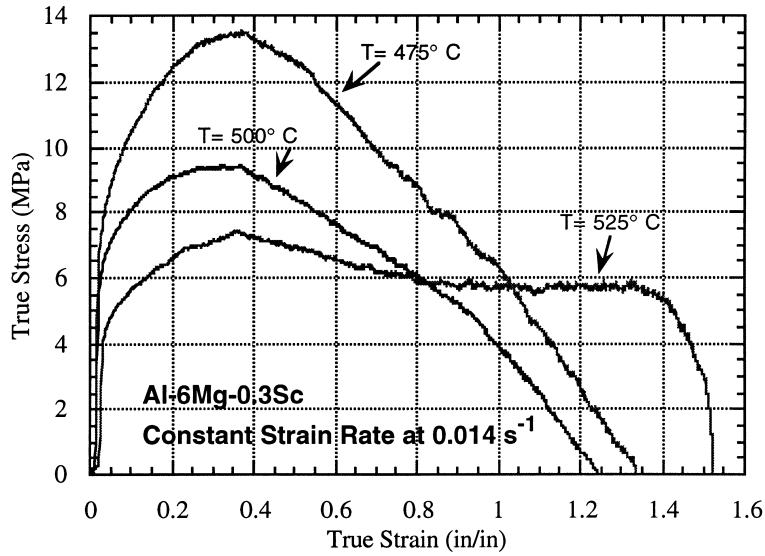
Fig. 17. True stress–strain curves obtained at a constant strain rate of $1.4 \times 10^{-2}\,\text{s}^{-1}$ at three different temperatures.

observed at 525°C is attributed to extensive grain coarsening at that temperature. So, it is proposed that the mechanism for superplasticity in the Al–6Mg–0.3Sc alloy is continuous recrystallization.

Continuous recrystallization during superplastic deformation has been observed in many aluminum alloys [17–23]. However, it has not been reported in Al–Mg based alloys [24]. In fact, Al 5083, which is a commercial Al–Mg alloy, was not found to deform by continuous recrystallization [25]. There exist several mechanisms describing continuous recrystallization [22, 26, 27]. In alloys which contain

a significant amount of coarse ($\sim$1 μm), uniformly-distributed, second-phase precipitates, continuous recrystallization is initiated at heavy deformation zones, e.g. at regions adjacent to the coarse precipitates (also known as particle stimulated nucleation, PSN [27]). A classical example is found in the Al–Cu–Zr alloys (Supral) in which Al$_2$Cu particles play a major role in nucleating new grains [18]. In contrast, in alloys which do not contain coarse second-phase precipitates, the mechanisms involve either the rotation [17] or switching [26] of subgrains, or both. Subgrain rotation, in turn, can result from
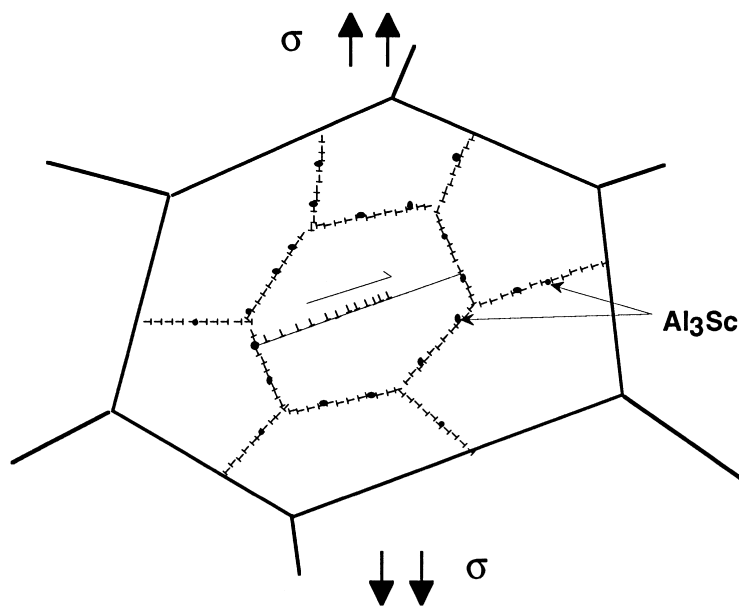

Fig. 18. The initial dislocation cells in cold rolled Al–6Mg–0.3Sc alloy quickly interact and annihilate with each other during preheating and form stable subgrains.

boundary sliding, or from dislocation slip on selected sets of slip systems within each grain. This leads to a gradual increase in the subgrain boundary angle and eventually into high-angled boundaries.

There is only a limited amount of coarse Fe- and Mn-rich precipitates [Fig. 10(b)] in the Al–6Mg–0.3Sc alloy. Also, the distribution of these precipitates was not uniform. The PSN mechanism is, thus, not expected to operate. It appears that, in the present case, continuous recrystallization can occur only through subgrain evolution. As discussed earlier, the initial structure of the alloy consists of dislocation cells (Fig. 8). During the preheat in each test, dislocations in the cell wall quickly interact and annihilate with each other; this leads to the formation of stable subgrains, as schematically illustrated in Fig. 18. Upon mechanical loading, dislocations with a favored Schmid factor begin to move across subgrains on selected sets of slip systems, resulting in an increase in the sub-boundary angle. These moving dislocations are expected to be pinned by Al_3Sc precipitates at the opposite subboundary. As this process continues, subgrain boundaries eventually convert to true high-angled grain boundaries. It is pointed out that it is difficult for this process to occur in other Al–Mg based alloys because of the absence of an effective subboundary pinning agent (i.e. Al_3Sc in the present case).

In the present Al–6Mg–0.3Sc alloy, the conversion from subgrain boundary to true high-angled grain boundary is believed to take place in the early stage of deformation. Data from Fig. 19 (strain rate sensitivity vs deformation strain) indicate that it may occur at a strain < 100%. Once high-angled boundaries are formed, grains are readily able to slide and grain boundary sliding begins to take over as dominant the deformation process. Also, as a
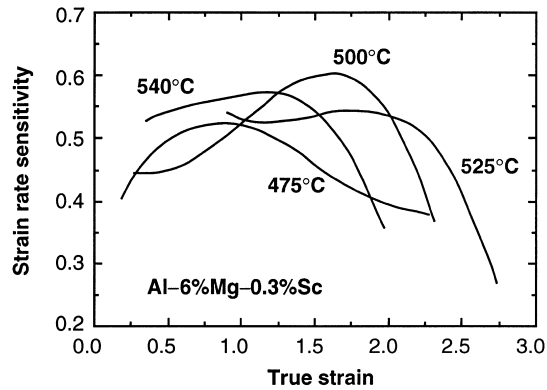

Fig. 19. Strain rate sensitivity of Al–6Mg–0.3Sc as a function of deformation strain at different temperatures.

result of the presence of Al_3Sc precipitates, grains remain fine and stable throughout deformation.

The accommodation of grain boundary sliding is usually associated with dislocation climb or glide, depending upon which one is rate controlling. That is,

$$\frac{1}{\dot{\varepsilon}_{overall}} = \frac{1}{\dot{\varepsilon}_{climb}} + \frac{1}{\dot{\varepsilon}_{glide}} \qquad (4)$$

where $\dot{\varepsilon}_{overall}$ is the overall deformation rate, and, $\dot{\varepsilon}_{climb}$, and $\dot{\varepsilon}_{glide}$ are dislocation climb and glide rates, respectively. In Al–Mg alloys, as a result of solute drag, intragranular dislocation glide has been recognized as the rate controlling process [13]. Fukuyo *et al.* [28] have proposed a model for grain boundary sliding accommodated by dislocation glide and predicted:

$$\dot{\varepsilon}_{gbs,glide} = A_{glide} \frac{D_{chem}}{d^2} \left(\frac{\sigma}{E} \right) \qquad (5)$$

where D_{chem} is the chemical diffusivity, and A_{glide} is a constant. According to the equation, the strain
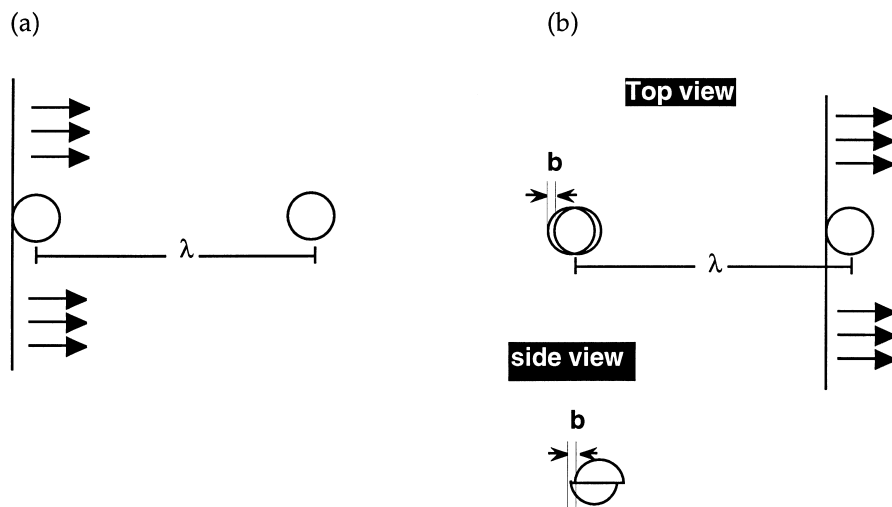
(a)

(b)

Fig. 20. Schematic illustration of particle shearing during dislocation glide through grains.

rate is linearly proportional to applied stress. In the model, the glide distance of dislocations was assumed to be similar to the grain diameter, i.e. there was no obstacle for gliding dislocations. However, in the present alloy, there is a uniform distribution of coherent Al_3Sc precipitates. These precipitates can act as obstacles for gliding dislocations but are readily shearable, as schematically illustrated in Fig. 20. Now, let us consider the shearing of Al_3Sc precipitates by a gliding dislocation.

The rate of dislocation glide, $\dot{\varepsilon}_{glide}$, is:

$$\dot{\varepsilon}_{glide} = \frac{v}{s} \qquad (6)$$

where v is the glide velocity, and s is the glide distance which, in the present case, is the interparticle spacing, λ. As shown in Fig. 20, the mechanical work (W) resulting from the dislocation glide is

$$W = \sigma \cdot \lambda \qquad (7)$$

where σ is the applied stress. The energy change, ΔE, caused by the shearing of the Al_3Sc particle, is approximately

$$\Delta E \sim 2\pi r \cdot b \cdot \gamma_{pm} \qquad (8)$$

where r is the radius of the precipitates, b is Burgers vector, and γ_{pm} is the Al_3Sc–Al interfacial energy. By combining equations (7) and (8), one obtains

$$\lambda = \frac{2\pi r \cdot b \cdot \gamma_{pm}}{\sigma} \qquad (9)$$

Inserting equation (9) into equation (6) and further assuming that $v = M \cdot \sigma$, where M is the glide mobility, it is readily shown that

$$\dot{\varepsilon}_{glide} = \frac{M}{2\pi r \cdot b \cdot \gamma_{pm}} \cdot \sigma^2 \qquad (10)$$

i.e. the deformation rate is proportional to the stress raised to a second power. In other words, the strain rate sensitivity value is 0.5. Interestingly, this is the same value as that predicted for the case of grain boundary sliding accommodated by the climb of dislocations [equation (1)].

In summary, superplasticity resulting from grain boundary sliding accommodated by dislocation glide across grain with a uniform dispersion of coherent precipitates can be described by the equation:

$$\dot{\varepsilon}_{gbs,glide} = \frac{M \cdot u}{2\pi r \cdot b \cdot \gamma_{pm}} \cdot \frac{1}{d} \cdot \sigma^2 \qquad (11)$$

$$= B_{gbs,glide} \cdot \left(\frac{1}{d}\right) \cdot \sigma^2 \qquad (12)$$

where d is the grain size and u is the unit displacement for grain boundary sliding. It is particularly

noted that the observed m values are indeed centered around 0.5 (Fig. 19).

5. SUMMARY

The microstructure and mechanical properties of a cold-rolled Al–6Mg–0.3Sc alloy have been characterized. The alloy exhibited superplasticity at relatively high strain rates ($\sim 10^{-2}\ s^{-1}$). At a strain rate of $10^{-2}\ s^{-1}$ there exists a wide temperature range (475–520°C) within which the tensile elongation is over 1000%. There also exists a wide strain rate range (10^{-3}–$10^{-1}\ s^{-1}$) within which the tensile elongation is over 500%. The presence of Sc in the alloy results in a uniform distribution of fine coherent Al_3Sc precipitates which effectively pin grain and subgrain boundaries during static and continuous recrystallization. As a result, the alloy retains its fine grain size ($\sim 7\ \mu m$), even after extensive superplastic deformation ($> 1000\%$). During deformation, dislocations with a high Schmid factor move across subgrains but are trapped by subgrain boundaries, as a result of the strong pinning of Al_3Sc. This process leads to the conversion of low-angled subgrain boundaries to high-angled grain boundaries and the subsequent grain boundary sliding, which produces superplasticity. In the present study, a model is also proposed to describe grain boundary sliding accommodated by dislocation glide across grains with a uniform distribution of coherent precipitates. It is noted that Al–6Mg–0.3Sc alloy is not susceptible to cavitation during superplastic deformation.

REFERENCES

1. Taleff, E. M., Henshall, G. A., Lesuer, D. R. and Nieh, T. G., in *Aluminum Alloys*, Vol. 1 — Their Physical and Mechanical Properties (ICAA4), ed. J. T. H. Sanders and J. E. A. Starke, The Georgia Institute of Technology Press, 1994, p. 338.
2. Taleff, E. M., Henshall, G. A., Lesuer, D. R., Nieh, T. G. and Wadsworth, J., in *Aluminum and Magnesium for Automotive Applications*, p. 125, edited by J. D. Bryant and D. R. White, The Minerals, Metals, and Materials Society, Warrendale, PA, 1996.
3. Taleff, E. M., Henshall, G. A., Lesuer, D. R., Nieh, T. G. and Wadsworth, J., in *Superplasticity and Superplastic Forming 1995*, ed. A. K. Ghosh and T. R. Bieler, The Minerals, Metals and Materials Society, Warrendale, PA, 1995, p. 3.
4. Sherby, O. D. and Wadsworth, J., *Prog. Mater. Sci.*, 1989, **33**, 166.
5. Ball, A. and Hutchinson, M. M., *Metal. Sci. J.*, 1969, **3**, 1.
6. Wang, J., Horita, Z., Furukawa, M., Nemoto, M., Tsenev, N. K., Valiev, R. Z., Ma, Y. and Langdon, T. G., *J. Mater. Res.*, 1993, **8**, 2810.

7. Wang, J., Horita, Z., Furukawa, M., Nemoto, M. and Langdon, T. G., *J. Mater. Res.*, 1996, **11**, 1880.

8. Blake, N. and Hopkins, M. A., *J. Mater. Sci.*, 1985, **20**, 2861.

9. Engler, O. and Tempus, G., in *Progress in Materials and Mechanics*, ed. T. Wang and T.-W. Chou, Peking University Press, 1996, pp. 423–428.

10. McQueen, H. J. and Kassner, M. E., in *Superplasticity in Aerospace II*, ed. T. R. McNelly and C. Heikkenen, The Minerals, Metals and Materials Society, Warrendale, PA, 1990, p. 77.

11. Sawtell, R. R. and Jensen, C. L., *Metall. Trans.*, 1990, **21A**, 421.

12. Nieh, T. G., Kaibyshev, R., Hsiung, L. M., Nguyen, N. and Wadsworth, J., *Scr. mater.*, 1997, **36**, 1011.

13. Taleff, E. M., Lesuer, D. R. and Wadsworth, J., *Metall. Mater. Trans.*, 1996, **27A**, 343.

14. McNelly, T. R. and Kalu, P. N., in *International Conference on Superplasticity in Advanced Materials (ICSAM-91)*, ed. S. Hori, M. Tokizane, and N. Furushiro, The Japan Society for Research on Superplasticity, Osaka, Japan, 1991, p. 413.

15. Nes, E., in *Superplasticity*, ed. B. Baudelet and M. Suery, Centre National de la Recherche Scientifique, Paris, 1985, p. 7.1.

16. Zedalis, M. S. and Fine, M. E., *Metall. Trans.*, 1986, **17A**, 2187.

17. Nes, E., *Metal Sci.*, 1979, **13**, 211.

18. Watts, B. M., Stowell, M. J., Baikie, B. L. and Owen, D. G. E., *Metal Sci.*, 1976, **10**, 189.

19. Wert, J. A., Paton, N. E., Hamilton, C. H. and Mahoney, M. W., *Metall. Trans.*, 1981, **12A**, 1267.

20. Lee, E. W., McNelley, T. R. and Stengel, A. F., *Metall. Trans.*, 1986, **17A**, 1043.

21. Gudmundsson, H., Brooks, D. and Wert, J. A., *Acta metall. mater.*, 1991, **39**, 19.

22. Lyttle, M. T. and Wert, J. A., *J. Mater. Sci.*, 1994, **29**, 3342.

23. Hamilton, C. H. and Ghosh, A. K., in *Metal Handbook*, Vol. 14, ed. S. L. Semiatin, ASM International, Metals Park, OH, 1988, p. 852.

24. Tallef, E. M., Henshall, G. A., Nieh, T. G., Lesuer, D. R. and Wadsworth, J., *Metall. Mater. Trans.*, 1997, in press.

25. Imamura, H. and Ridley, N., in *International Conference on Superplasticity in Advanced Materials (ICSAM-91)*, ed. S. Hori, M. Tokizane and N. Furushiro, The Japan Society for Research on Superplasticity, 1991, p. 453.

26. Ashby, M. F. and Verrall, R. A., *Acta metall.*, 1973, **21**, 149.

27. Humphreys, F. J., *Acta metall.*, 1977, **25**, 1323.

28. Fukuyo, H., Tsai, H. C., Oyama, T. and Sherby, O. D., *ISIJ Int.*, 1991, **31**, 76.